Original Research

Dual-Route Preparation of Fe_2O_3 Nanostructures (Green and PLD) for Superior H_2S Detection Sensitivity

Estabraq A. Jadaan [1], Noor S. Saleh [1], Othman Abed Fahad [1,*]

[1] Ministry of Education, Direction of Education in AL-Anbar, Iraq

* Correspondence: othmanabad2@gmail.com; ORCID: 0000-0002-7073-7994

Received: November 8, 2025; Accepted: February 10, 2026

Abstract: Green synthesis is becoming increasingly important as an environmentally friendly alternative to conventional production processes due to its growing industrial applications. In this study, aloe Vera leaf extracts were used to synthesize Fe_2O_3 nanoparticles. The micro powder was converted to nanoparticles after mixing with aloe Vera, followed by calcination and annealing. Pulsed laser deposition (PLD) was then used to deposit Fe_2O_3 nanoparticles on glass substrates at laser energies of 200 and 400 mJ. The structural, morphological, energy band gap and hydrogen sulfide sensitivity of the Fe_2O_3 nanoparticles were studied. The Fe_2O_3 nanoparticles exhibited a polycrystalline structure, and structural results derived from the Scherrer equation, AFM, and FESEM indicated that the grain size increased with increasing laser energy, resulting in densely packed, spherical-like nanoparticles. UV-Vis spectroscopy results show that the energy gap decreases from 2.3 eV to 2 eV with increasing laser power. This sensor was developed to detect H_2S gas sensitivity at different temperatures: Room temperature, 60 °C, and 100 °C. The Fe_2O_3/glass sample showed the highest sensitivity (88%) to H_2S gas at laser energy of 200 mJ and an operating temperature of 100 °C. The sensitivity of the material decreased as the laser energy increased to 400 mJ. However, the response and recovery times for both laser energies were average and decreased with increasing operating temperature.

Keywords: green method; PLD method; Fe_2O_3 nanoparticles; H_2S gas sensor

1. Introduction

In recent decades, a variety of materials, including organic and inorganic conductive materials, such as metal oxide semiconductors, have been used to develop gas sensors [1]. Iron oxide (Fe_2O_3), with a band gap of 2.2 eV, is one of the most important transition metal oxides. It has received significant attention due to its positive intrinsic physical and chemical properties, including low cost, high stability under various conditions, and environmental friendliness [2]. These characteristics allow for a wide range of uses for Fe_2O_3 nanostructures, including gas sensors [3]. A wide range of gases and vapors, including NO_2, NH_3, CO, H_2S, C_3H_7OH, C_2H_5OH, and CH_3OH, can be detected by α-Fe_2O_3 nanostructures acting as a sensor [4,5]. Controlling public safety and protecting the environment both depend on accurate monitoring of gas exposure levels. The development of gas sensor properties, such as low cost, quick reaction, high sensitivity, ease of use, good time recovery, and selectivity, is currently the focus of significant attention [6,7]. The use of metal oxide semiconductors as sensor materials is essential to gas sensing. Target gas molecules interact with oxygen compounds like O− on the surface of the sensor material; this changes the sensor's resistance and electrical conductivity, allowing us to detect the gas by measuring the electrons that are released or captured during this interaction [8,9]. One of the most important features of semiconductor gas sensors is their high sensitivity, high selectivity, and low cost,

enabling rapid on-site detection [10]. The colorless gas known as hydrogen sulfide (H_2S) is extremely dangerous, combustible, and smells like rotten eggs. It can be created by the decomposition of organic materials and human and animal waste, including sewage and trash dumps, and it is found naturally in natural gas and crude petroleum. Since H_2S is heavier than air, it can be gathered in enclosed, low-lying spaces with inadequate ventilation, such as underground [11]. Sewer pipes, manholes, basements, and electrical/telephone vaults [12]. There are several techniques used to prepare Fe_2O_3 films, including pulsed laser deposition (PLD) [13], reverse micro emulsion method [14], thermal evaporation [15], and green method [16]. The green technique is a good way to get low-cost, high-quality results. However, as Figure 1 illustrates, this approach takes more time than physical and chemical approaches [17]. In the quickly expanding field of environmentally friendly industrial technology, there is a greater need for green synthesis of nanoparticles. In the quickly expanding field of environmentally friendly industrial technology, there is a greater need for green synthesis of nanoparticles [18]. Because it may be utilized to create vast quantities of contamination-free nanoparticles with a well-defined size and morphology, the green technique is more significant than conventional methods. Therefore, new techniques for creating ecologically acceptable, low-cost, ambient-temperature-formed nanoparticles are being considered [19,20]. Previous studies on Fe_2O_3-based H_2S sensors mostly focus on a single synthesis method, without systematically comparing how different fabrication routes affect structural features and sensing performance. As a result, the connection between preparation strategy and sensor behavior remains unclear, which this work aims to clarify.

This work aims to suggest a dependable method for making iron oxide nanoparticles that are similar in size and to improve understanding of how these nanoparticles are created and grow. Although Fe_2O_3-based materials have been widely investigated for H_2S gas sensing, most reported studies rely on a single fabrication method, leaving the role of synthesis strategy in governing sensing performance insufficiently clarified. This work addresses this gap by employing two fundamentally different preparation routes—green synthesis and pulsed laser deposition—and directly comparing their structural characteristics and H_2S sensing behavior under identical conditions. The results provide clear insight into how the fabrication route influences surface activity and sensor response, establishing a rational basis for optimizing Fe_2O_3-based gas sensors.

2. Fe_2O_3 synthesis

Nanostructured Fe_2O_3 was synthesized using Aloevera extract. Two to three Aloevera leaves were washed thoroughly with distilled water, and the gel was collected, finely ground with an electric blender while gradually adding 10 mL of distilled water, then heated for 10 min and filtered. A 0.1 M solution was prepared by dissolving 3 g of ferrous sulfate heptahydrate ($FeSO_4{\cdot}7H_2O$, Panreac AppliChem, Spain) in 300 mL of deionized water and stirred for 10 min at room temperature to achieve homogeneity. Then, 20 mL of Aloevera extract was added and continuously stirred until the solution turned yellow. Sodium hydroxide (1 M, BDH, Spain) was added drop wise until the solution turned gray after 25 min of continuous stirring. The mixture was centrifuged at 5000 rpm for 12 min, and the supernatant was washed repeatedly with deionized water. The resulting black-red nanoparticles were dried at 100 °C for 5 h and calcite at 400 °C for 4 h. The obtained nanoparticles were pressed into a pellet with a thickness of 1 cm and width of 2 cm, which was used as a PLD target. Fe_2O_3 thin films were deposited using a Nd:YAG laser (λ = 1064 nm, pulse duration 10 ns, repetition rate 10 Hz) with a target-substrate distance of 5 cm in a background of high-purity oxygen (10 mTorr) at a substrate temperature of 200 °C for 30 min, producing a uniform nanostructured film of ~150 nm thickness. The sensor was fabricated on a glass substrate in the Al/Fe_2O_3/glass configuration, with aluminum contacts deposited by thermal evaporation (Edwards E306A) under vacuum (~10.5 Pa). Structural characterization was performed using X-ray diffraction (Philips PW 1710, Cu Kα, λ = 1.5406 Å), atomic force microscopy, and FESEM (NOVA NANOSEM 450) to study morphology and particle size, while UV-Vis spectroscopy (Shimadzu UV-3600) was used to examine optical properties. Gas sensing

measurements were carried out in a controlled chamber equipped with temperature and humidity control, with sensor resistance recorded using a digital multimeter (UNI-T UT81B) connected to a PC. H_2S gas (47.7 ppm) was generated by diluting a certified 100 ppm H_2S cylinder with dry air using mass-flow controllers at a total flow of 200 sccm. Sensitivity (S) was calculated as $S = \frac{R_{gas}-R_{air}}{Rair} \times 100\%$, where R_{gas} and R_{air} are the sensor resistances in H_2S and air, respectively.

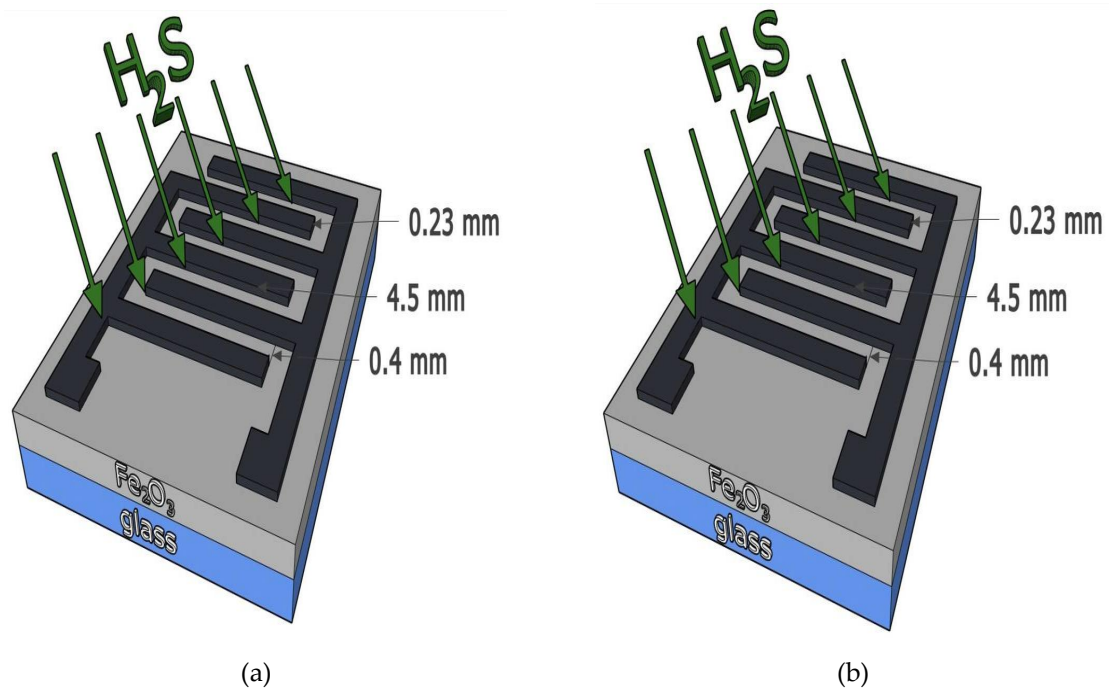

(a) (b)

Figure 1. (a) Shows the synthesis of Fe_2O_3 nanoparticles; (b) Applied gas sensor.

3. Result and discussion

3.1. Structure properties

3.1.1. XRD analysis

X-ray diffraction (XRD) was performed to investigate the structural properties of Fe_2O_3 nanoparticles synthesized using two different laser energies. The patterns, recorded from 20° to 80° 2θ (Figure 2), show well-defined peaks at 24.35°, 33.27°, 41.10°, 43.27°, 49.39°, 54.09°, and 57.22°, corresponding to the (012), (104), (110), (113), (116), (018), (214), and (300) planes, in agreement with JCPDS card No. 33–0664, confirming the formation of the α- Fe_2O_3 phase and high phase purity. These findings are comparable to those of Ahmed et al. [21]. We note from the figure that when the laser power increases, the crystallinity of the material increases from 12.7 to 22.3 nm.

The FWHM of the main peak at 33.27° decreased from 1.43 to 0.69 as laser energy increased from 200 mJ to 400 mJ, indicating improved crystallinity. The calculated crystallite size increased from 12.7 nm to 22.3 nm. This enhancement is attributed to higher thermal energy at elevated laser powers, promoting atomic diffusion, grain growth, and reduced lattice defects. The improved crystallinity and larger crystallites are expected to enhance charge transport and provide stable adsorption sites, positively influencing the gas-sensing performance of the sensor.

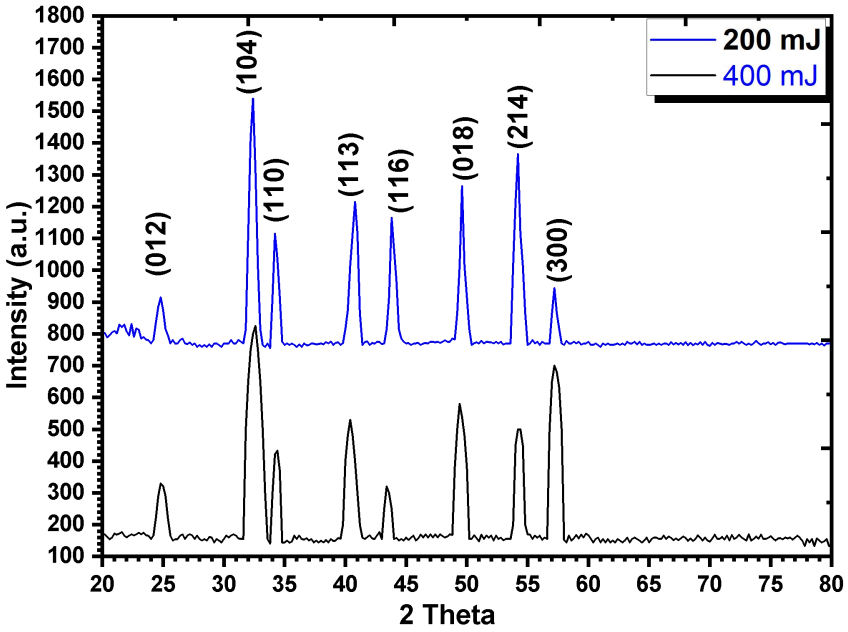

Figure 2. Displays X-ray diffraction patterns of Fe_2O_3 at laser energy (200, mJ 400 mJ).

3.1.2. Atomic force microscope (AFM)

Atomic force microscope (AFM) image of a Fe_2O_3 sample at various laser energy are displayed in Figure 3. The images demonstrate that as the laser energy rose, the grain size grew from 15 nm to 32 nm and the roughness dropped from 4.10 nm to 3.24 nm. The average particle size is known to be significantly influenced by laser energy. The size of the nanoparticles grows with laser energy. This outcome is comparable to the findings of Jihad [12]. As the laser energy increases as Figure 3(b), the particles' kinetic and thermal energy also increases, which raises the impact velocity of the nanoparticles and provides them with substantial surface mobility [22]. As a result, in order to lower the system's high surface energy, big clusters of particles form; consequently, the clusters cause the nanoparticles' overall grain size to grow [23,24]. The increase in grain size with rising laser energy is accompanied by a decrease in surface roughness due to enhanced atomic mobility and grain coalescence. At higher laser energies, smaller grains merge into larger, more uniform grains, filling surface valleys and smoothing the film. This results in larger crystallites with a more even surface, which can improve charge transport and provide stable adsorption sites for gas sensing.

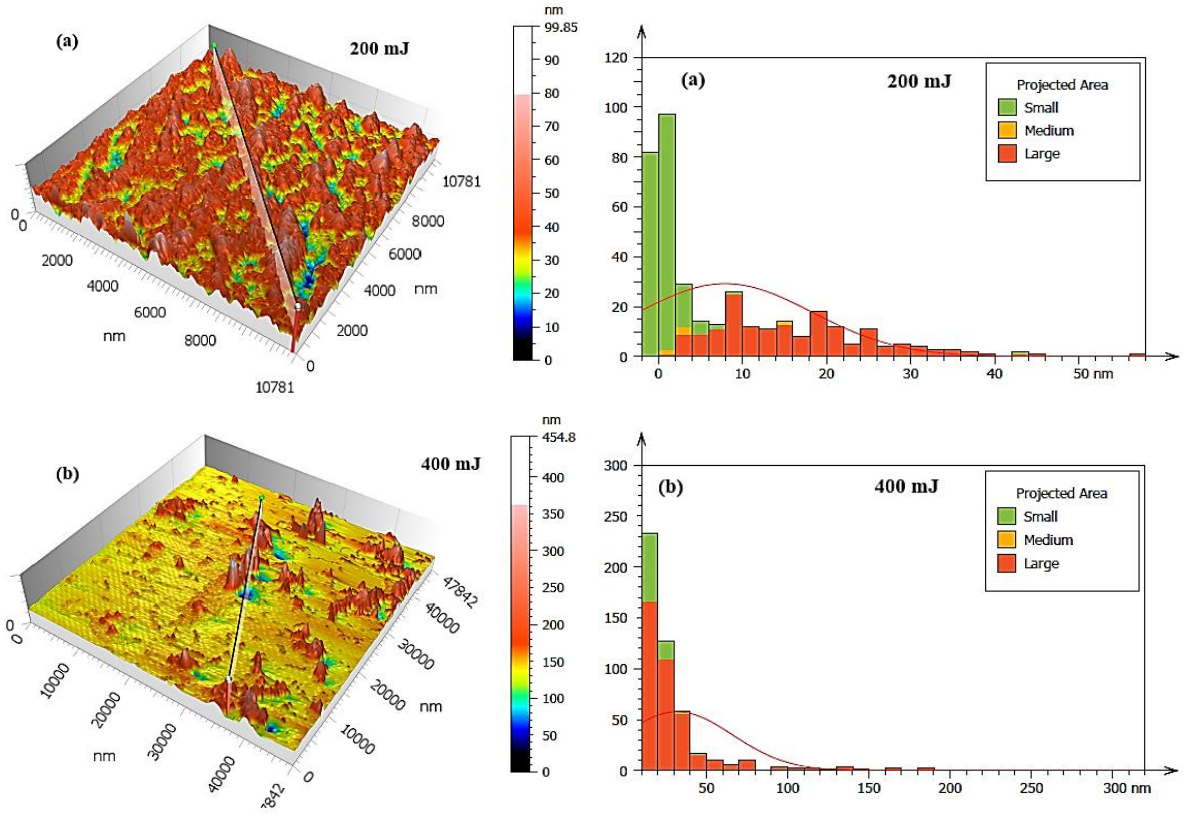

Figure 3. AFM topography of Fe_2O_3 thin film deposited by PLD at laser energy. (a) 200 mJ; (b) 400 mJ.

3.1.3. FESEM analysis

FESEM pictures were utilized to examine the material's morphology, including the size and form distribution of the particles, as well as the chemical makeup of the thin Fe_2O_3 layers made using two distinct methods, as seen in Figure 4. According to the images shown, the Fe_2O_3 nanoparticles feature smooth spherical grains. In detail, the spheres in Figure 4(a) appear wrinkled, dense, and tightly packed. This observation may indicate active surface interaction and charge separation for gas sensing function. As the laser energy increases as Figure 4(b), the crystallinity of the material improves, forming a somewhat open and interconnected network. By Image j program, the average diameter of the Fe_2O_3 spheres deposited at laser energies of 200 mJ and 400 mJ was found to be 42 nm and 60 nm, respectively.

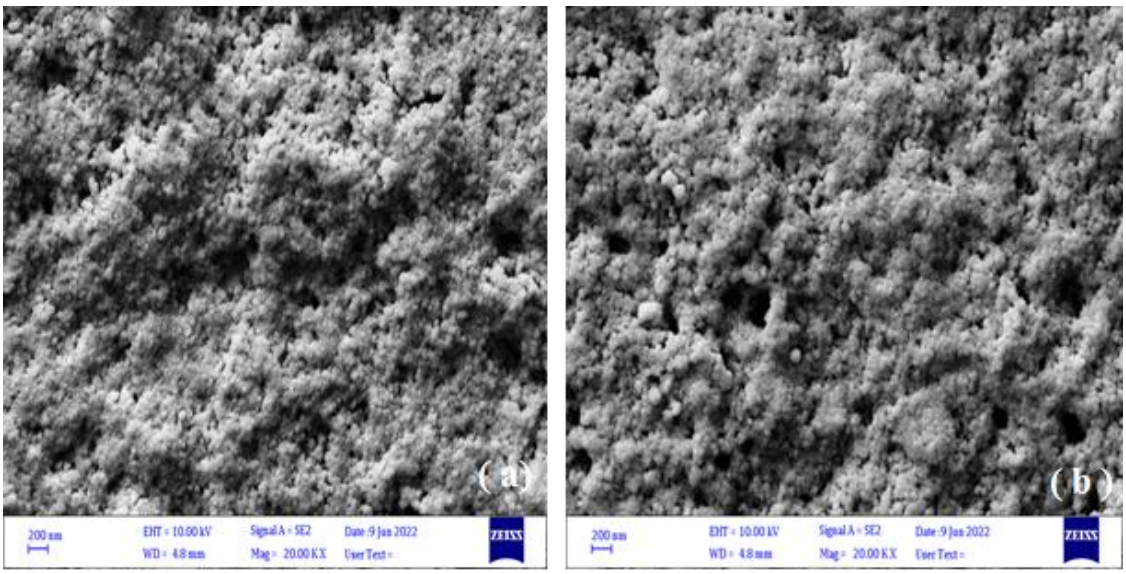

Figure 4. FESEM image of Aloevera-modified Fe_2O_3 nanoparticles at laser energy. (a) 200 mJ; (b) 400 mJ.

3.2. Optical properties

The optical band gap of iron oxide films at laser energies of 200 and 400 mJ was estimated from the following relationship [25]:

$$\alpha h\nu = (h\nu - Eg)^{1/2} \quad (1)$$

The above relationship was used to find the band gap values and energy types for the prepared films, which had a direct-type band gap energy allowed. Figure 5 showed an energy gap of 2.3 eV which is good consistent with Jihad [12, 26] and the figure shows that the band gap value decreases with increasing laser energy to 400 mJ, to about 2 eV. The decrease in the band gap is attributed to the increase in crystal size [27, 28], which can be understood by comparing the FESEM and AFM results.

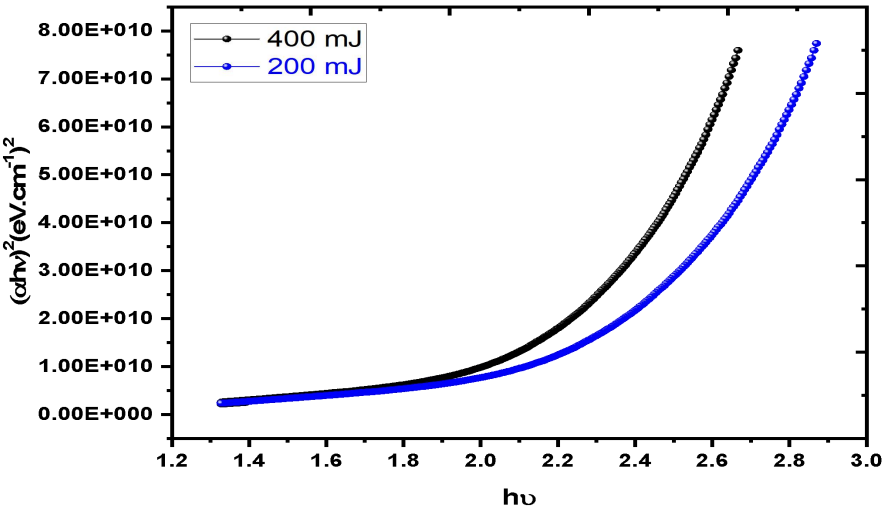

Figure 5. Displays energy gap of Fe_2O_3 at laser energy 200 mJ, and 400 mJ.

3.3. H_2S gas sensor

Figure 6 shows the variation of the sensor's current (A) of H_2S agents time (s) at different temperature (RT, 60 ºC and 100 ºC). The plots exhibit a distinct external behavior, which is

characteristic of metal oxide sensors. The increase in current with increasing operating temperature of the a-Fe_2O_3 sensor indicates the semiconducting nature of the metal oxide, i.e., thermal energy excites electrons from the valence band to the conduction band [29]. When H_2S gas, a reducing gas, is applied to the Fe_2O_3 sample, the current increases and then rapidly decreases when the gas is turned off, indicating that the sample exhibits n-type conductivity. The electrical conductivity of Fe_2O_3 samples is affected by the absorption of oxygen in the surrounding atmosphere. In addition, the absorption of oxygen ions removes conduction electrons, reducing the conductivity of the iron. The mechanism of action of the Fe_2O_3 nanosensor is that when exposed to a reducing gas such as H_2S at any temperature, it induces a reaction between the target gas and the surface oxygen molecules of the Fe particles, reducing the concentration of −O− ions and increasing the electron concentration. In polycrystalline materials with many grain boundaries, the charge state change occurs only at the grain boundaries or porous surfaces [30]. Consequently, the electron transport properties change significantly due to gas adsorption. Figure 6 shows the current-time relationship for a Fe_2O_3 film at 200 mJ laser energy at RT, 60 °C, and 100 °C. Table 1 show that the prepared film exhibits a sensitivity of 62% at RT. The sensitivity increases with the gradual increase in operating temperature, reaching about 88% at 100 °C, the optimum temperature. This is likely due to the significant increase in the response rate of the target gas surface. Figure 6(b) shows the sensitivity of iron oxide to hydrogen sulfide gas at laser energy of 400 mJ. A sensitivity of 29% was achieved at RT, which is lower than that achieved at laser energy of 200 mJ. This decrease in sensitivity may be attributed to the increased grain size, as shown by the SEM and AFM results. It is known that increasing the particle size leads to a decrease in the surface-to-volume ratio, which leads to a decrease in the number of gas absorption sites.

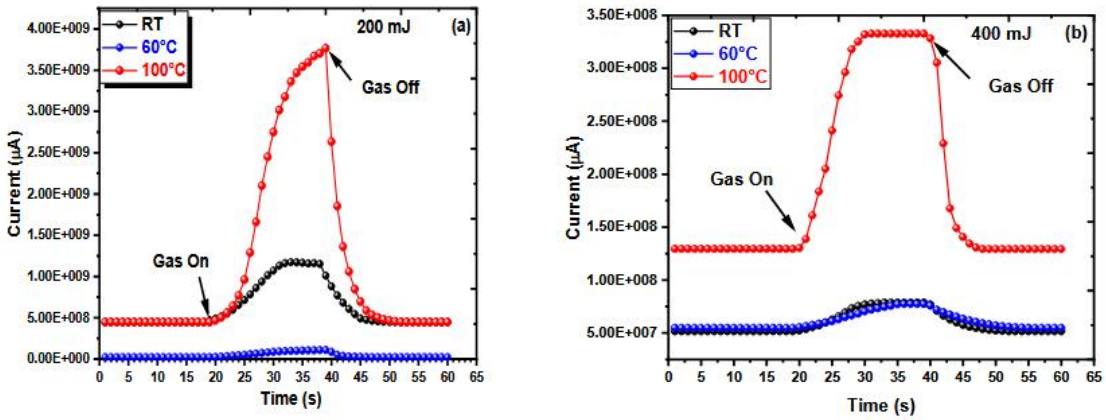

Figure 6. Current of H_2S versus time of Fe_2O_3 at laser energy 200 mJ, and 400 mJ. (a) 200 mJ; (b) 400mJ.

Figure 7(a) shows the relationship between grain size of AFM and sensitivity of H_2S gas at laser energy of 200 and 400 mJ at different temperatures. Particle size can affect the response of a material by influencing the chemical adsorption of the gas to the surface. Previous experiments have shown that the smaller the particle size, the higher the specific surface area. This is likely due to the possibility of increasing the effective surface area, which increases the number of adsorption and active sites, thus increasing the reactions that occur at the surface of the material [31]. Therefore, we observe a decrease in the sensitivity of the material as the grain size of the material increases, as mentioned in Table 1. We also observe an increase in the sensitivity of the material with increasing temperature. This is a general characteristic of semiconductors, where the conductivity of the material increases with increasing temperature. The reduced grain size also increases the boundary of the particles, providing a large surface area for oxygen and oxygen adsorption [32, 33]. Thus, the large difference in barrier and resistance can enhance the reaction at low temperatures, which contributes to obtaining good sensitivity at room temperature. Figure 7(b,c) shows the changes in the response and recovery time of the H_2S gas sensor based on Fe_2O_3

nanostructures at laser energy 200 and 400 mJ with different operating temperatures at a gas concentration of 47.7 ppm. The figure shows that as the operating temperature increases, the response and recovery times decrease. This may be due to several reasons, mainly because adsorption and desorption are thermal reactions that are sensitive to temperature [34]. In addition, at higher operating temperatures, electrons transfer between the conduction band and the Fermi level of the surface, which enhances the adsorption reaction and shortens the response and recovery times. Table 1 shows that at an operating temperature of 100 °C, the best response times for laser energies of 200 and 400 mJ are 8.0 and 6.5, respectively.

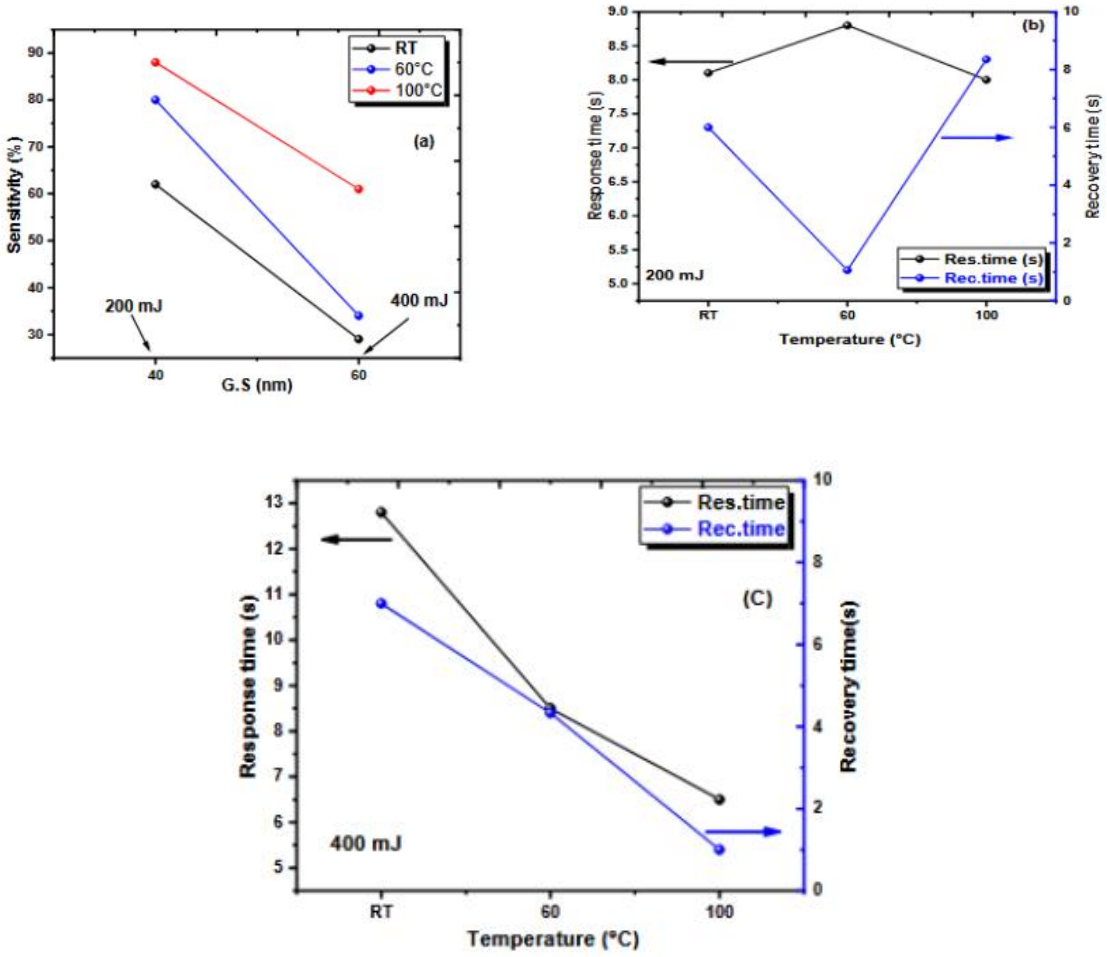

Figure 7. (a) Shows the relationship between grain size of AFM and sensitivity; (b and c) shows the changes in the response and recovery time of the H_2S gas sensor.

Table 1. Sensitivity parameter of H_2S gas sensor at 200 mJ and 400 mJ.

Fe_2O_3	Sensor working temperature (°C)			Sensitivity (%)			Response time (s)			Recovery time (s)		
200 mJ	RT	60	100	62	80	88	8.1	8.8	8.0	7.3	5.2	8.3
400 mJ	RT	60	100	29	34	61	12.8	8.5	6.5	10.8	8.4	5.4

The PLD-prepared sensor demonstrates faster response and recovery, while the green-synthesized sensor shows comparable performance to typical Fe_2O_3-based H_2S sensors, highlighting the effect of fabrication method on sensor behavior.

The present study is limited to laboratory-based H_2S sensing measurements under controlled conditions and a restricted set of test parameters. Further investigations on long-term stability and environmental effects are required to fully assess the practical applicability of the proposed sensors.

4. Conclusion

Two different methods (green and PLD) were used to prepare Fe_2O_3 nanostructures. The X-ray diffraction (XRD) pattern showed that all films were polycrystalline in nature and that the average crystallite size increased with increasing laser energy. Morphological studies using FE-SEM and Atomic Force Microscopy (AFM) revealed a smooth surface, high density, and large crystallite aggregates in the form of nanoparticles. The average particle size was found to increase with increasing laser power. With increasing laser power, a red shift was observed in the optical analysis, along with a decrease in the energy band gap pattern. A thin Fe_2O_3 sensor film was prepared, and it showed a significant dependence on the laser power value and increasing operating temperature. The sensitivity and response time decreased significantly with increasing operating temperature.

Acknowledgments: The authors thank the plasma laboratory at the College of Science, University of Anbar.

Availability of Data and Materials: All data are available if requested by the reviewers and for external data inferred within the manuscript they cited in the references.

Funding: This research received no external funding.

Author Contributions: EAJ and OAF, conceptualization, project administration, resources, visualization; EAJ , conceptualization, data curation, formal analysis, investigation, methodology, software, supervision, validation, visualization, writing—original draft, writing—review and editing; OAF and NSS , investigation, methodology, supervision, validation, writing—original draft, writing—review and editing. All authors have read and approved the final manuscript. All authors contributed to editorial changes in the manuscript. All authors have participated sufficiently in the work and agreed to be accountable for all aspects of the work.

Ethics Approval: Ethics approval not required.

Conflicts of Interest: The authors declare no conflict of interest.

References

1. Mohammed, A.S.; Fahad, O.A. Sensitivity enhancement for NO_2 gas sensor based on Alq_3:TiO_2. In: Proceedings of the AIP Conference Proceedings; 2372, 040008 (2021); https://doi.org/10.1063/5.0065972.
2. Zolghadr, S.; Khojier, K.; Kimiagar, S. Ammonia Sensing Properties of α-Fe_2O_3 Thin Films During Post-Annealing Process. *Procedia Materials Science* 2015, 11, 469–473. https://doi.org/10.1016/j.mspro.2015.11.058
3. Huo, L.H.; Li, Q.; Zhao, H.; et al. Sol-gel route to pseudocubic shaped α-Fe_2O_3 alcohol sensor: Preparation and characterization. *Sensors and Actuators B: Chemical* 2005, 107, 915–920. https://doi.org/10.1016/j.snb.2004.12.046
4. Bandgar, D.K.; Navale, S.T.; Mane, A.T.; et al. Ammonia sensing properties of polyaniline/α-Fe_2O_3 hybrid nanocomposites. *Synthetic Metals* 2015, 204, 1–9. https://doi.org/10.1016/j.synthmet.2015.02.032
5. Jiang, Z.X.; Li, J.; Aslan, H.; et al. A high efficiency H_2S gas sensor material: Paper like Fe_2O_3/graphene nanosheets and structural alignment dependency of device efficiency. *Journal of Materials Chemistry A* 2014, 2, 6714. https://doi.org/10.1039/C3TA15180H
6. Cuong, N.D.; Khieu, D.Q.; Hoa, T.T.; et al. Facile synthesis of α-Fe_2O_3 nanoparticles for high-performance CO gas sensor. *Materials Research Bulletin* 2015, 68, 302–307. https://doi.org/10.1016/j.materresbull.2015.03.069

7. Dehkordi, H.A.; Mokhtari, A.; Soleimanian, V.; et al. High Sensitive α-Fe_2O_3 Nano-structured Gas Sensor Fabricated through Annealing Technique for Detecting Ethanol. Social Science Research Network 2023; Pre-publication. https://ssrn.com/abstract=4367915
8. Barsan, N.; Koziej, D.; Weimar, U. Metal oxide-based gas sensor research: How to? *Sensors and Actuators B: Chemical* 2007, 121, 18–35. https://doi.org/10.1016/j.snb.2006.09.047
9. Kim, H.J.; Lee, J.H. Highly sensitive and selective gas sensors using p-type oxide semiconductors: Overview. *Sensors and Actuators B: Chemical* 2014, 192, 607–627. https://doi.org/10.1016/j.snb.2013.11.005
10. Gao, X.; Chen, Y.; Xu, P.C.; et al. γ-Fe_2O_3-Based MEMS Gas Sensor for Propane Detection. *Electronics* 2025, 14, 1050. https://doi.org/10.3390/electronics14051050
11. Hanfoosh, S.; Mohammed, A.S. High-Performance Visible-Light Photodetectors Based on CeO_2-Doped V2O5 Nanostructure: Optoelectronic Characterization. Plasmonics 2025; June 25-27, 2025. /doi.org/10.1007/s11468-025-03196-w.
12. Jihad, G.H. Synthesis and Characterization of α-Fe_2O_3 Nanoparticles Prepared by PLD at Different Laser Energies. *Iraqi Journal of Science* 2021, 62, 3901. https://doi.org/10.24996/ijs.2021.62.11.11
13. Liang, S.; Li, J.P.; Wang, F.; et al. Highly sensitive acetone gas sensor based on ultrafine α-Fe_2O_3 nanoparticles. *Sensors and Actuators: B. Chemical* 2017, 238, 923–927. https://doi.org/10.1016/j.snb.2016.06.144
14. Fahad, O.A.; Mohammed, A.S.; Salih, E.Y.; et al. Perpendicular sheet-like alignment of a self-driven MoS_2/Si heterostructure for Vis-NIR wavelength detection. *Nanoscale* 2025, 17(30), 17795–17802. https://doi.org/10.1039/D5NR02331A
15. Jiang, S.X.; Peng, L.H.; Guo, R.H.; et al. Preparation and characterization of Fe_2O_3 coating on quartz fabric by electron beam evaporation. *Ceramics International* 2016, 42, 19386–19392. https://doi.org/10.1016/j.ceramint.2016.09.111
16. Mohammed, A.M.; Saud, W.M.; Ali, M.M. Green Synthesis of Fe_2o_3 Nanoparticles Using Olea Europaea Leaf Extract and Their Antibacterial Activity. *Digest Journal of Nanomaterials and Biostructures* 2020, 15, 175–183. https://doi.org/10.15251/DJNB.2020.151.175
17. Shaheen, A.; Haija, M.A.; Chamakh, M.; et al. Fabrication and characterization of poly(vinyl alcohol)—Glycerol—Spinel ferrites flexible membranes. *Journal of Applied Polymer Science* 2020, 137(24), 48821. https://doi.org/10.1002/app.48821
18. Hamid, N.M.; Abed, H.A.; Fahad, O.A. Evaluation of Antibacterial Effects of Silver Nanoparticles Synthesized via Pulsed Laser Ablation at Different Laser Energies. *Lasers in Manufacturing and Materials Processing* 2025, 12, 488–497. https://doi.org/10.1007/s40516-025-00295-8
19. Goutham, S.; Kaur, S.; Sadasivuni, K.K.; et al. Nanostructured ZnO gas sensors obtained by green method and combustion technique. *Materials Science in Semiconductor Processing* 2017, 57, 110–115. https://doi.org/10.1016/j.mssp.2016.09.037
20. Korbekandi, H.; Iravani, S.; Abbasi, S. Production of nanoparticles using organisms. *Critical Reviews in Biotechnology* 2009, 29, 279–306. https://doi.org/10.3109/07388550903062462
21. Hilo, D.H.; Ismail, A.H.; Al-Garawi, Z.S. Green Synthesis of A-Fe_2O_3 from Ginger Extract Enhanced the Potential Antioxidant Activity against DPPH. *Al-Mustansiriyah Journal of Science* 2022, 33, 64. https://doi.org/10.23851/mjs.v33i4.1208
22. Myerlas, R. Key Parameters of Pulsed Laser Deposition for Solid Electrolyte Thin Film Growth. *International Journal of Advances in Engineering and Technology* 2017, 10, 46–51. http://www.ijaet.org/media/5I37-IJAET1001126-v10-iss1-pp46-51.pdf
23. Happy; Mohanty, S.R.; Lee, P.; et al. Effect of deposition parameters on morphology and size of FeCo nanoparticles synthesized by pulsed laser ablation deposition. *Applied Surface Science* 2006, 252, 2806–2816. https://doi.org/10.1016/j.apsusc.2005.04.026
24. Mohammed, A.; Abdulghani, S. *Dig. J. Nanomater. Biostruct.* 2022, 17.
25. Zhang, D.Z.; Wu, J.F.; Li, P.; et al. Room-temperature SO_2 gas-sensing properties based on a metal-doped MoS_2 nanoflower: An experimental and density functional theory investigation. *Journal of Materials Chemistry A* 2017, 5(39), 20666–20677. https://doi.org/10.1039/C7TA07001B
26. Mohammed, A.S. *J. Phys. Conf. Ser.* 2021.
27. Mazhir SN, Abdalameer NK, Yaaqoob LA, Hammood JK. Bio-Synthesis of (Zn/Se) Core-Shell Nanoparticles by Micro Plasma-Jet Technique. Int. J. Nanosci., 2022; 21, 51, 2250041. https://doi.org/10.1142/S0219581X22500417.

28. Ayesh, A.I.; Haija, M.A.; Shaheen, A.; et al. Spinel ferrite nanoparticles for H_2S gas sensor. *Applied Physics A* 2017, 123(11), 682. https://doi.org/10.1007/s00339-017-1305-7
29. Jaffer, Z.J.; et al. *J. Phys. Conf. Ser.* 2021.
30. Li, Y.; Lu, Y.L.; Wu, K.D.; et al. Microwave-assisted hydrothermal synthesis of copper oxide-based gas-sensitive nanostructures. *Rare Metals* 2020, 40, 1477–1493. https://doi.org/10.1007/s12598-020-01557-4
31. Hou, S.H.; Zhuang, X.M.; Fan, H.D.; et al. Grain Boundary Control of Organic Semiconductors via Solvent Vapor Annealing for High-Sensitivity NO_2 Detection. *Sensors* 2021, 21, 226. https://doi.org/10.3390/s21010226
32. Liu, X.H.; Zhang, J.; Guo, X.Z.; et al. Porous α-Fe_2O_3 decorated by Au nanoparticles and their enhanced sensor performance. *Nanotechnology* 2010, 21, 095501.
33. Righettoni, M.; Amann, A.; Pratsinis, S.E. Breath analysis by nanostructured metal oxides as chemo-resistive gas sensors. *Materials Today* 2015, 18, 163–171. https://doi.org/10.1016/j.mattod.2014.08.017